Materials Today Chemistry 26 (2022) 101146

Contents lists available at ScienceDirect

Materials Today Chemistry

journal homepage: www.journals.elsevier.com/materials-today-chemistry/

# Evaluation of the degradation of the graphene-polypropylene composites of masks in harsh working conditions

I. Torres [a], B. González-Tobío [a], P. Ares [b], J. Gómez-Herrero [b], F. Zamora [a, *]

[a] Departamento de Química Inorgánica, Institute for Advanced Research in Chemical Sciences (IAdChem) and Condensed Matter Physics Center (IFIMAC), Universidad Autónoma de Madrid, 28049, Madrid, Spain
[b] Departamento de Física de La Materia Condensada and Condensed Matter Physics Center (IFIMAC), Universidad Autónoma de Madrid, 28049, Madrid, Spain

ARTICLE INFO

*Article history:*
Received 8 January 2022
Received in revised form
8 August 2022
Accepted 13 August 2022
Available online xxx

*Keywords:*
Graphene
Polypropylene
Non-woven
Face masks
Coronavirus

ABSTRACT

The recent COVID-19 outbreak has led health authorities to recommend at least the use of surgical masks, most preferably respirators (FFP2 or KN95), to prevent the spread of the virus. Non-woven fabrics have been chosen as the best option to manufacture the face masks, due to their filtration efficiency, low cost, and versatility. Modifying the mask filters with graphene has been of great interest due to its potential use as antibacterial and virucidal properties. Indeed, some companies have commercialized face masks in which graphene is coated and/or embedded. However, the Canadian sanitary authorities advised against using the Shandong Shengquan New Materials Co. graphene masks because of the possibility of pulmonary damage produced by graphene inhalation. Thus, we have analyzed the stability of the graphene filter of these masks and compared it with two other commercially available graphene mask filters, evaluating the morphological and spectroscopical change of the fibers, as well as the particles released during the endurance tests. Our work introduces the necessary tools and methodology to evaluate the potential degradation of face masks under extreme working conditions. These methods complement the present standard tests ensuring the security of the new filters based on composites or nanomaterials.


## 1. Introduction

Viruses can be described as supramolecular containers with typical sizes ranging from tens to hundreds of nanometers carrying genetic information inside. After infection, they disrupt the host cellular machinery to propagate themselves [1,2]. For efficient transmission, viruses must be stable enough to protect ribonucleic acids, but adaptable sufficient to release their genome at the right time and place [3]. The main challenge in a pandemic scenario is to control respiratory virus spread, which supposes an enormous health and socioeconomic threat [4]. The propagation vector of viruses is often air-suspended micrometric droplets spread through the airways of the infected person [5–7]. This aerosol can be inhaled by someone else or placed on surfaces, giving rise to their propagation to another host with the appropriate humidity conditions [8]. In the case of the SARS-CoV-2 (Severe Acute Respiratory Syndrome Coronavirus, strain 2), it is already accepted that it is mainly transmitted through saliva and snot droplets from infected individuals [6,7]. Therefore, it is recommended or, in many countries an obligation, to use masks to reduce the risk of transmission, particularly indoors. Masks are used to prevent both the expulsion and the entry of pathogens [2,9] and, as the General Council of Official Associations of Pharmacists explains, the droplets get trapped in the masks, wetting them and rendering them useless. Despite different technologies to obtain fabrics, non-woven (where the fibers are bonded together by chemical, mechanical, heat, or solvent treatments) is the best for filters and mask fabrication due to its better filtration efficiency, low cost and versatility. Many polymers such as polyethylene (PE), poly(-ethyleneterephthalate) (PET), poly(butyleneterephthalate) (PBT), polystyrene (PS), polyurethane (PUR), polyamide (PA), and polypropylene (PP) are used to produce non-woven fabrics, being the last one the most commonly used material to manufacture prophylactic masks [10]. Moreover, non-woven spunbond-melt-blown-spundbond (SMS) PP filters present fine mesh structural parameters, excellent filtration properties, thermal insulation, and sorption capacity, giving as a result good permeability and high efficiency [11,12]. On top of that, parameters of the non-woven PP

* Corresponding author.
*E-mail address:* felix.zamora@uam.es (F. Zamora).

https://doi.org/10.1016/j.mtchem.2022.101146

filters such as pore size, fiber diameter, and areal density can be modulated for different applications [10].

Recently nanomaterials, particularly 2D materials, have been used in nanofiltration to fabricate membranes [13–15] and face masks [16,17]. 2D materials are nanomaterials that present unprecedented physical, electronic, and chemical properties due to electron confinement in two dimensions. In some cases, graphene has been proposed to complement the filter barrier due to its suggested potential antibacterial and virucidal properties [18–20]. Furthermore, in response to the global COVID-19 pandemic, recent studies suggest that graphene can be used in virus detection [21], air filters [22], and protective clothing [23,24]. Indeed, different methodologies have been developed for face mask modification with graphene [25–28]. As a result, some companies have developed and commercialized protective materials such as fabrics, wipes, air filters, or face masks in which graphene is coated and/or embedded.

However, in the last few months, the possibility of toxicity produced by graphene inhalation set off the alarms when the Canadian sanitary authorities recommended avoiding using face masks with graphene. This fact highlighted the necessity of an appropriate analysis of the security of the masks that contain nanomaterials before arriving at the market. Nowadays, the Canadian sanitary authorities have permitted the sale of some graphene-based masks, but only those which have been confirmed their security. Inhalation of graphene oxide (GO), a derivative of graphene, has been found to cause adverse effects on the lungs [29]. Nevertheless, some studies indicate that long periods (6 h/day, 20 days) of continuous inhalation of graphene (0.0099 mg/day, 0.198 mg accumulated) have no adverse effects on the lungs [30,31]. The use of new materials to improve the properties of actual personal protective equipment may imply the actualization of the quality standards, to ensure the security of the new products. The tests and requirements to be passed for the commercialization of personal protective equipment are included in the UNE-EN 149:2001 + A1 standard. This standard focuses on particle filtration, inhalation resistance, and thermal stability tests but does not consider tests of possible degradation of the material. There are alternative reported methods for pre-certification screening, but they all focus on particle filtration [32–35].

In this study, we provide a new methodology that combines different technologies to complement the actual standard tests to ensure the security of the filters modified with nanomaterials. Therefore, we decided to study the stability of the Biomass Graphene KN95 Particulate Respirator (BG-KN95) masks from Shengquan Group, a surgical graphene mask (SHC) from Guangzhou Nan Qi Xing Nonwoven, a graphene surgical masks filters ($G^+$) for cotton facial masks from Directa Plus and a standard FFP2 mask from Zhejiang Aopeng Industry and Trading, to determine the potential degradation and morphological stability of these filters under extreme working conditions. As all masks are commercial, they have all passed the requirements of the UNE-EN 149:2001 + A1 standard, so we propose additional tests to this standard to observe the possible degradation of the fibers and to be able to distinguish specific masks from others.

## 2. Experimental section

### 2.1. Breathing simulation test

Airflow of 60 L/min was introduced in a three-neck bottle with Milli-Q water to simulate human breath. A sensor allowed controlling the air humidity, which was set to 100%, as so in extreme conditions. The airflow left the bottle passing through five filters of 66.5 $cm^2$ each, enclosed between two stainless steel cones. Once the filters were crossed, the air was forced to bubble 50 mL of Milli-Q water, collecting the possible detached particles (ultra-pure water to avoid potential interferences in the carbon detection and simulate the environment of human lungs). The experiment was carried out at ambient temperature (*ca.* 25 °C) for 8 h, the maximum recommended time for using face masks.

### 2.2. Ultrasonic bath treatment

For the harsh working conditions test, five filters of 197 $cm^2$ were introduced in a 1 L bottle with 300 mL of Milli-Q water. The glass container was sonicated in an ultrasonic bath at 380 W, 37 kHz, and 50 °C for 8 h, the maximum wearing time of the masks recommended by the manufacturer.

### 2.3. Graphene suspensions preparation

Graphene suspensions were prepared following the method reported by Zamora et al. [36]. In a typical synthesis, 50 mg of graphite powder was put on a 20 mL vial with 10 mL of a THF/water (4:1) mixture. The mixture was sonicated for 90 min at 380 W and 37 kHz. Then, the resulting black suspension was centrifuged at 550 g for 60 min and the supernatant was recovered.

## 3. Results and discussion

Among the characteristics of face mask filters, their stability understood as their capacity to last without changes in properties or to withstand wear and tear, is crucial to avoiding health problems derived from inhalation. In the case of face masks containing graphene, the stability of the composite forming the fibers is essential. The BG-KN95 masks (SI for additional details) have four layers: a 60 $g/m^2$ (60G) anti-sticking PP non-woven fabric, a filtration PP melt-blown filter, and a graphene@polypropylene (G@PP) composite non-woven filter, and a 30 $g/m^2$ (30G) anti-sticking non-woven fabric. SHC masks contain outer dust waterproof PP non-woven fabric layer, a filtration PP melt-blown filter, and a G@PP composite non-woven fabric as the inner layer. $G^+$ filters are produced according to a proprietary patented methodology [13] in which the PP fibers of the filter are coated with physically exfoliated graphene. Finally, FFP2 masks contain three layers: spundbond PP non-woven as outer and inner layers and meltblown PP non-woven layer as intermediate layer.

To study the fiber degradation and the possible liberation of graphene, particles, or molecules during face mask use, as a first experiment, we designed a breathing simulator (schematic and photography in Figs. 1a and S1, respectively). The system works by introducing an airflow in a three-neck bottle that contains Milli-Q water and a sensor to control the air humidity. The airflow gets out of the bottle and passes through five enclosed filters, each one between two stainless steel cones. After crossing the filters, the air is forced to bubble Milli-Q water, collecting the possible detached particles (ultra-pure water is selected to avoid possible interferences in carbon detection and simulate the environment of human lungs). The safety of the BG-KN95 Shengquan masks was questioned because of their G@PP filter, which contains 1% by weight of graphene, so we decided to examine this filter in deep as well as another two types of graphene masks and a standard FFP2 mask. We separated all the mask filters and focused our interest on testing and characterizing the G@PP one in BG-KN95 and SHC masks, all the filters in $G^+$, and the inner spundbond PP non-woven layer in a commercial FFP2 mask. The filters were manipulated by wearing aseptic nitrile gloves to prevent any contamination. The experiment was carried out at ambient temperature (*ca.* 25 °C), and the air flow was set at 60 L/min,

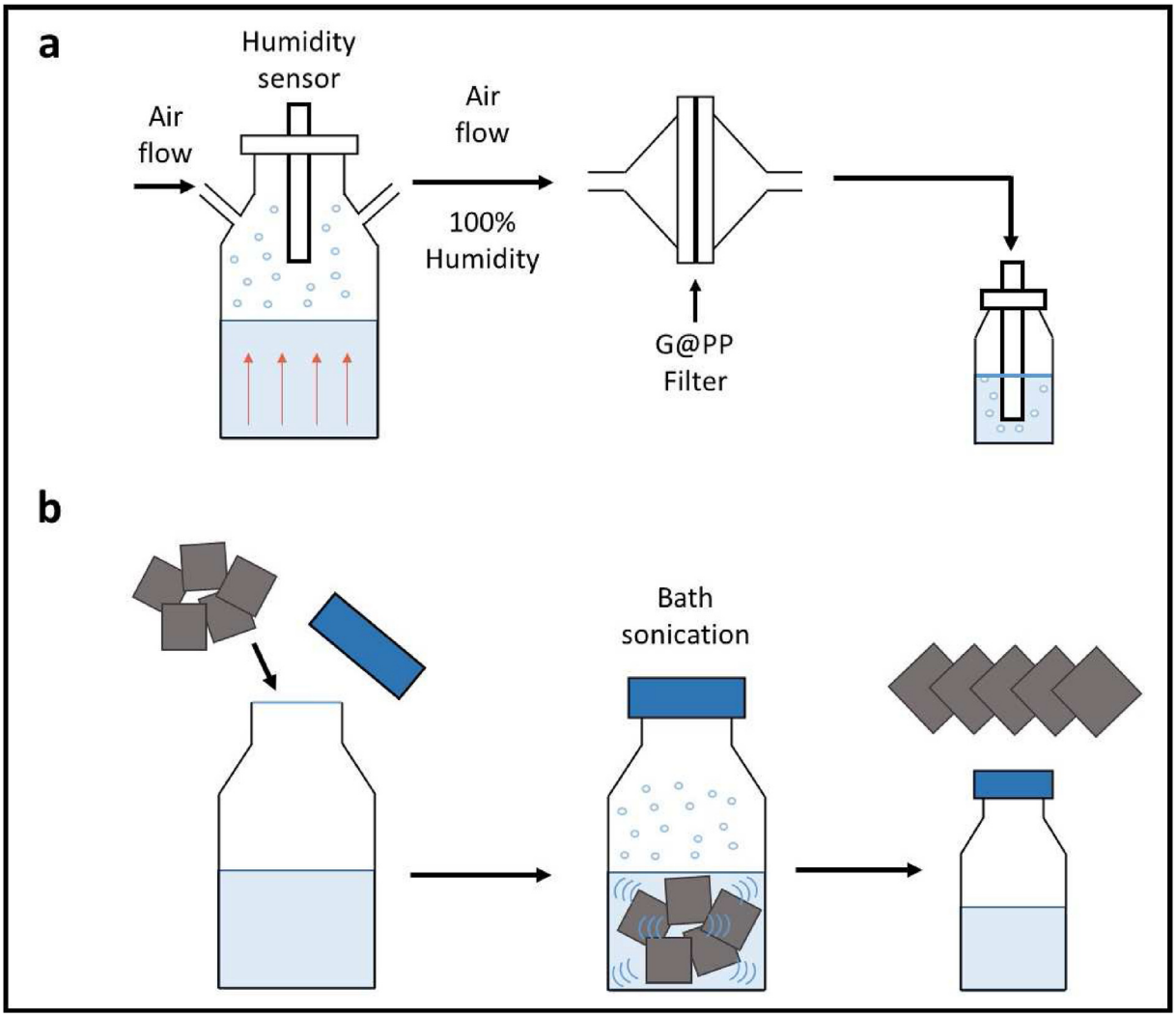


**Fig. 1.** Diagrams of the endurance tests. a) Scheme of the breath simulator system used in the study. The simulation consists of a flow of humid air passing through the mask filter, and the possible residue is collected in Milli-Q water in a bottle. b) Scheme of the system to expose the filters to harsh working conditions. The mask filters are sonicated in Milli-Q water for 8 h, subjecting them to high stress.

approximately the value of the adult human breath during exercise [37]. To extreme the working conditions, the experiment was carried out by setting the relative humidity of the air flow at 100%. We passed the humid air flow through the filters for 8 h, since this is the maximum recommended time for the use of face masks. Finally, all the particles detached during the experiment were collected in a bottle with 50 mL of Milli-Q water.

To ensure the resistance and stability of the face mask filters, we toughened further the experimental conditions for the second experiment. Thus, the filters were exposed to harsh working conditions to determine any potential degradation or morphological changes of the filters, fibers, or graphene composites. The experiment was carried out by introducing five filters in a bottle with 300 mL of Milli-Q water. The glass container was sonicated in an ultrasonic bath at 380W, 37 kHz, and 50 °C for 8 h (maximum time of use recommended by the manufacturer company). With this treatment, we estimate the applied energy to be about 1600 J over the filters (SI for additional details). To put this figure in perspective, we can compare it with the energy cost of breathing. According to Choi et al. [38], "the energy cost for a single inhalation varies with the mask type in a range between 0 and 10 mJ". From this value, we can estimate an upper bound of 288 J for the total energy cost of breathing during exercise in 8 h (SI for additional details), more than 5 times less energy than the applied in the ultrasonic bath treatment.

### 3.1. Fibers endurance analysis

After the tests, the residues collected in Milli-Q water and the filters were analyzed separately. The fiber morphology was characterized optically and by Scanning Electron Microscopy (SEM), both before and after exposure of the filters to the working conditions. In the optical images of pristine BG-KN95 G@PP filters, it can be seen that the fibers are very homogeneous and present a diameter size in the range of 20–30 μm (Fig. S2). Besides, SEM images confirm the diameter size and show some roughness and little particles on the surface of pristine BG-KN95 G@PP fibers (Figs. 2a and S3). These small particles show sizes in the range of 0.5–3.5 μm. In the same way, SHC G@PP fibers and the $G^+$ filter were analyzed. In optical images, SHC G@PP fibers are highly uniform and exhibit a diameter size in the order of 30–40 μm (Fig. S4). SEM images confirm the diameter size and show particles in the fiber surface similar to those seen on the BG-KN95 masks (Figs. 2b and S5). The fibers of the $G^+$ filters display diameter sizes between

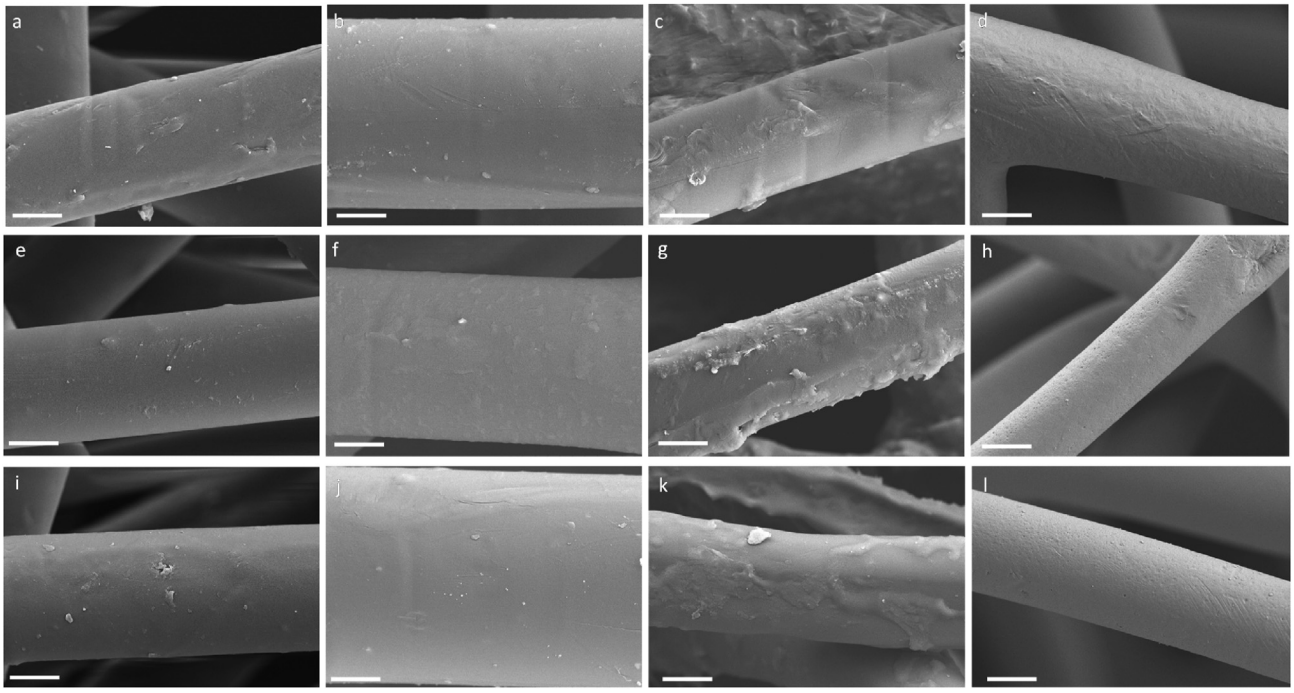


**Fig. 2.** Morphological characterization of the fibers. a-d) SEM images of pristine fibers (a) BG-KN95 G@PP, (b) SHC G@PP, (c) $G^+$ and d) FFP2. e-h) SEM images of fibers after breathing test conditions e) BG-KN95 G@PP, (f) SHC G@PP, (g) $G^+$, and (h) FFP2. i-l) SEM images of fibers after harsh working conditions test. (i) BG-KN95 G@PP, (j) SHC G@PP, (k) $G^+$ and (l) FFP2. Scale bars of 10 μm.

20 and 30 μm. As far as they are coated with physically exfoliated graphene, the fibers present a higher graphene load on the surface of the fibers and particles with larger lateral dimensions (Figs. 2c and S6-7). Additionally, FFP2 fibers were also analyzed by SEM microscopy. The diameter of the fibers is homogeneous and in a range of 15–25 μm (Figs. 2d and S8). The fibers were also characterized after exposure to the breathing simulation test and the harsh working conditions. After the tests, the optical microscope images of the G@PP fibers display the same disordered fiber network and diameter size as the pristine G@PP (Figs. S9–11). Furthermore, the particles over the surface, as seen by SEM, present a similar morphology and size to the particles of pristine G@PP fibers (Figs. 2 and S12-14). Similarly, no changes were observed in the network or the fiber size of the FFP2 fibers (Fig. S15). Thus, no changes in the morphology, size, or roughness of the fibers tested were observed.

The nature of the graphene and polypropylene present in the fibers was analyzed by Raman spectroscopy. The Raman spectrum of the pristine BG-KN95 G@PP composite filter (after subtracting the PP spectrum) reveals the typical graphene bands, the D mode at 1350 $cm^{-1}$, the G mode at 1586 $cm^{-1}$, and the 2D mode at 2700 $cm^{-1}$ (Fig. 3a, black line) [39], with an appearance that suggests that the graphene present in the G@PP fibers of the BG-KN95 was obtained by Liquid Phase Exfoliation (LPE) [40]. Due to the solvent, strain, doping, and edge effects caused during the LPE process, the Raman spectrum of LPE graphene is more difficult to analyze than graphene obtained by mechanical exfoliation [41]. The appearance of the D band suggests that graphene presents defects, and the intensity ratio between the signals 2D and G indicates that this structure consists of few-layer graphene, with an upper bound of *ca.* 5 layers based on the shape of the 2D peak [42]. Similarly, the Raman spectrum of pristine SHC G@PP fiber (after subtracting the PP spectrum) was analyzed, showing the characteristically reduced graphene oxide (rGO) bands, displaying the D and G modes in the same Raman shift as graphene but with the ratio $I_D/I_G$ increased (Fig. 3b, black line). Additionally, the 2D mode presents lower intensity due to the interlayer stacking produced in GO reduction [43,44]. On the other hand, the graphene of the $G^+$ filters is obtained by physical exfoliation, so the Raman spectrum of these filters shows the typical G and 2D bands of graphene, and it does not present the D band because of the absence of defects (Fig. 3c, black line) [39]. The nature of the PP of the FFP2 filter was also evaluated by Raman. The spectrum displays the typical bands of PP between 500 and 1500 $cm^{-1}$ and from 2600 to 3000 $cm^{-1}$ (Fig. 3d, black line). Moreover, the nature of the fibers materials was also analyzed after running the stability tests. The PP spectra of all of the filters do not present significant differences before and after the tests, suggesting that these working conditions do not produce any change in the PP structure (Figs. 3d and S16). Additionally, changes in the graphene structure were analyzed, finding that the spectra of the graphene of the BG-KN95 and the rGO of the SHC remains unaltered after the tests (Fig. 3a and b). However, the spectra of the $G^+$ filters after the experiments reveal the appearance of the D mode, which indicates that these procedures induce defects in the structure of the physical exfoliated graphene of the $G^+$ filters (Fig. 3c).

Raman mappings were acquired on single G@PP fibers before and after the stability tests in order to evaluate any change in the distribution of graphene. The G@PP composites may present graphene on the surface but also inside the G@PP fibers. For this reason, the Raman mapping was collected in the XZ plane. Moreover, the coated fibers of the $G^+$ filters may only present graphene on the surface of the PP fiber. Using the typical bands of both materials, we generated images that reveal the distribution of the graphene particles along the fibers, both on the surface and inside the pristine G@PP fibers. The pristine G@PP fibers of the BG-KN95 masks present a homogeneous distribution of graphene particles and the whole fiber, with characteristic lengths ranging between 0.5 and 3.5 μm (Fig. S17a), in agreement with the SEM data (Figs. 2a and S3). Furthermore, we also observe no significant differences

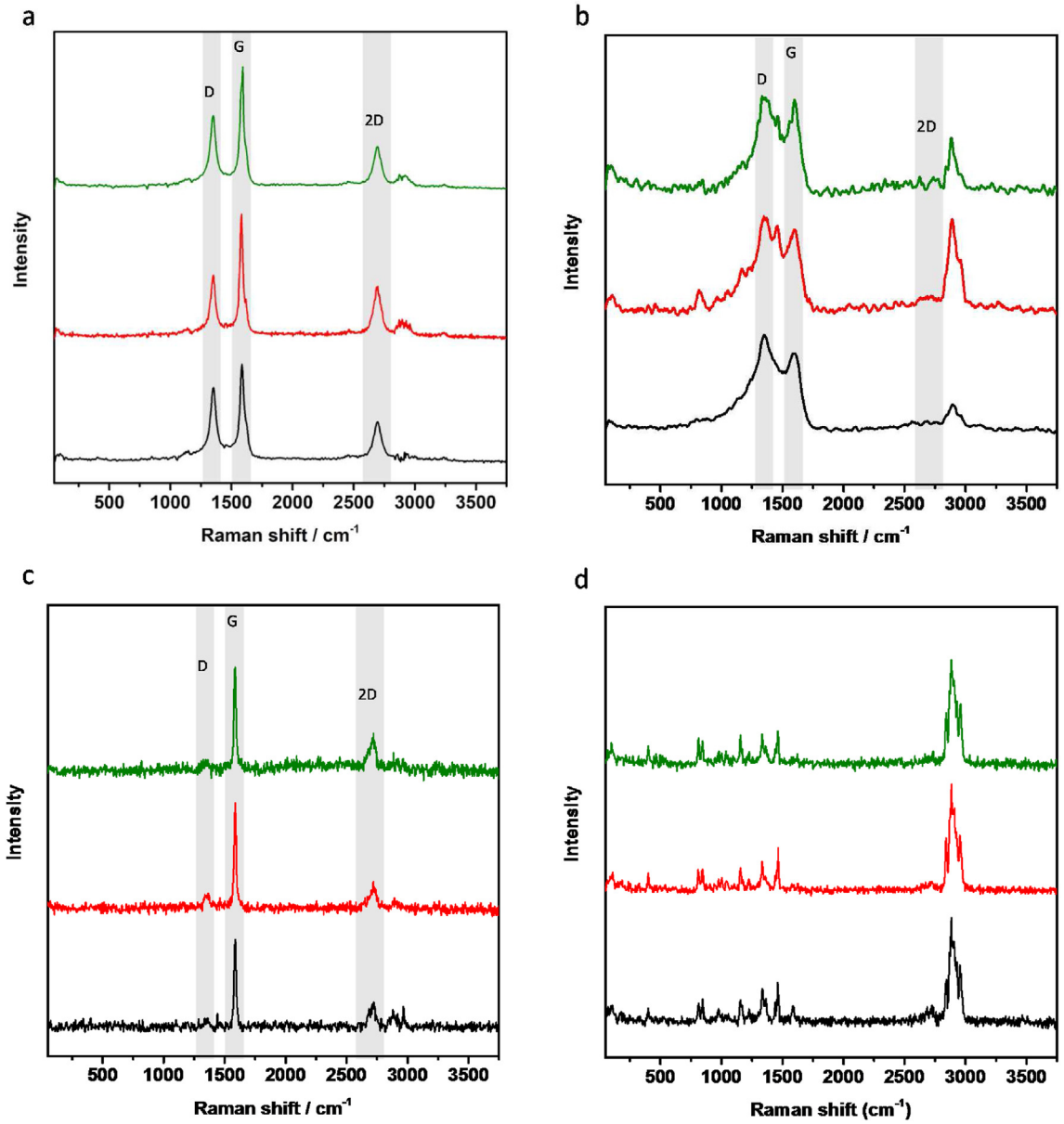


**Fig. 3.** Raman characterization of filters. a) Raman spectra of graphene bands present on BG-KN95 G@PP fibers. b) Raman spectra of rGO bands present on SHC G@PP fibers. c) Raman spectra of graphene bands present on $G^+$ fibers. d) Raman spectra of polypropylene bands on FFP2 fibers. In all cases, pristine fibers (black line), breathing test (red line), and harsh working conditions test (green line).

between the number of graphene particles on the surface and inside the fibers, suggesting that the preparation method creates a homogeneous graphene distribution along with the whole fiber. In the same way, the G@PP fibers of the SHC masks show a homogeneous distribution of rGO particles with sizes up to 2 μm (Fig. S17b). Besides, the number of particles on the surface and inside the fibers is also very similar, indicating the homogeneous distributions of the nanomaterial. However, in this case, the amount of particles is clearly lower than in the G@PP filters of the BG-KN95.

Finally, the Raman mapping images of the fibers of the $G^+$ filters present particles only on the surface because the modification method is based on coating. The graphene particles of the surface-displayed lengths around 10 μm (Fig. S17c).

After the breathing simulation experiment and the harsh conditions test, we carried out the same analysis on the G@PP fibers. The graphene particles are also homogeneously distributed along the fibers and present sizes in the same range shown in the SEM images (Fig. S17). Moreover, in the filters of BG-KN95 and SHC there are no substantial differences in the number of graphene particles on the surface and inside, as seen in the pristine fibers. Therefore, the Raman mapping analysis suggests that the G@PP filters do not modify the nature and number of graphene particles after undergoing the tests.

### 3.2. Residues content analysis

In view of these results, we analyzed the residues collected in the Milli-Q water to explore particle detachment from the masks. Graphene and PP are carbon-based materials, so we measured the total organic carbon (TOC) of the residue samples to analyze their carbon content. The total carbon (TC) was determined via ultra-high temperature oxidation into $CO_2$ and analyzed with an

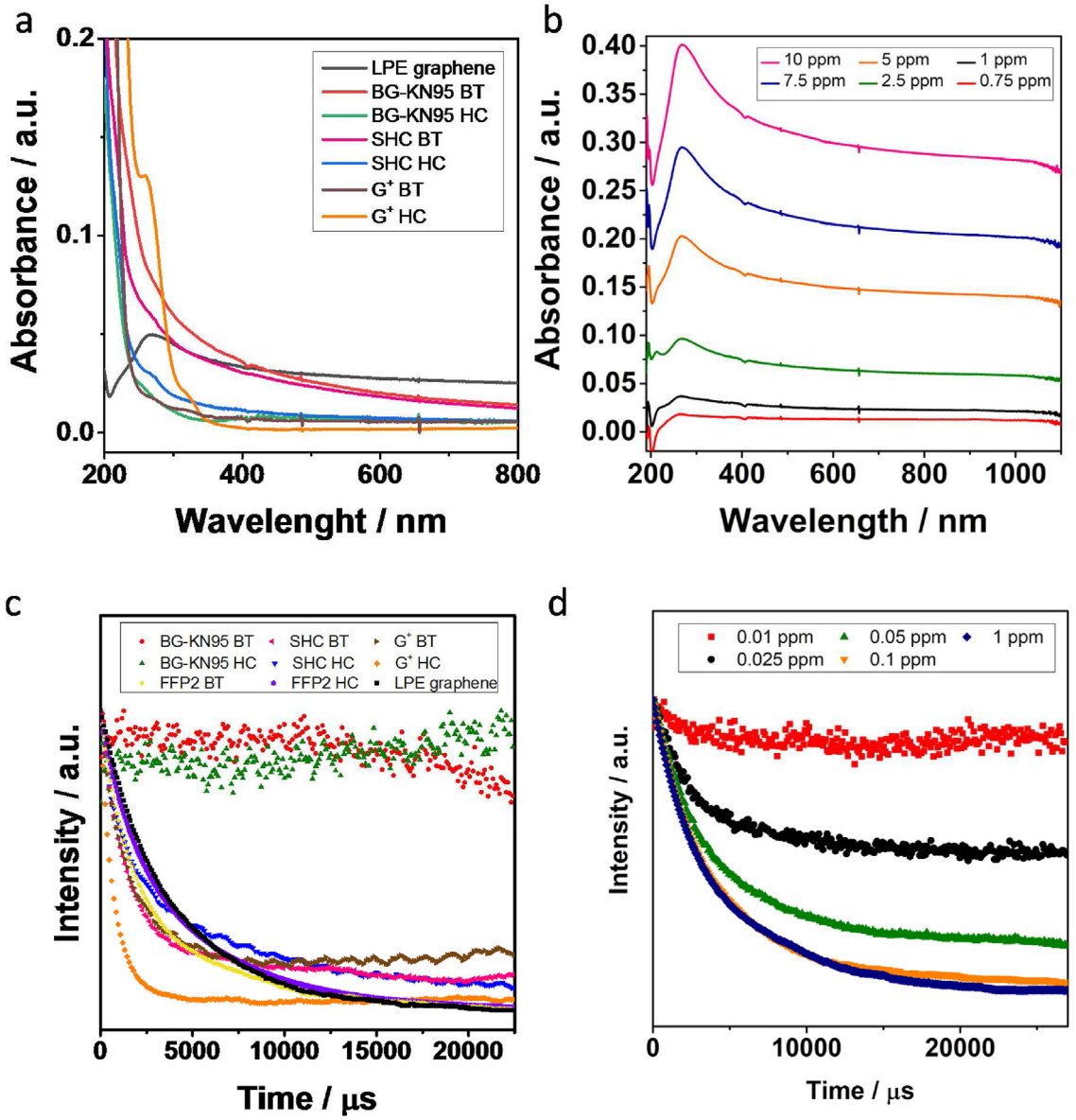


**Fig. 4.** Residues and detection limit analysis. a) UV–vis spectra of the residues collected from the breathing simulation test and harsh working conditions test. b) UV–vis spectra of the LPE graphene suspension at different concentrations, from more concentrated (top) to less concentrated (bottom). c) DLS signals the residues collected from the breathing simulation test and harsh working conditions test. d) DLS measurements of the graphene suspension prepared by LPE at different concentrations, from more concentrated (bottom) to less concentrated (top).

infrared gas detector. The inorganic carbon (IC) was determined by acidifying the medium to produce $CO_2$, and the organic carbon (OC) was calculated by subtracting the IC from the TC. In this technique, the IC only includes carbonate, bicarbonate, and dissolved carbon dioxide [45]. The Milli-Q water used in this experiment was also characterized as a control, finding that all the carbon values (TC, TIC, and TOC) were below 0.25 ppm, the detection limit of the equipment. The collected residue of the breathing test for BG-KN95 G@PP fibers presented 6 mg/L of TC, being all organic carbon. Taking into account that the measurement is done with 100 mL and considering the area of the G@PP filters used in the experiment and that each face mask has a filter area of 197 $cm^2$, this result indicates that each mask releases *ca.* 355 μg of organic carbon. The collected residue of the harsh conditions test displays 3.4 mg/L of TC, being all organic carbon also in this case. This measurement was done using 100 mL too, but the whole residue of the five face masks filter was collected in 300 mL of Milli-Q water, so the organic carbon release in the second test is 204 μg for each mask. Besides, SHC G@PP filters present 9.2 mg/L and 12 mg/L for breathing test and harsh conditions, respectively. This indicates that each filter releases 545 μg of organic carbon after the breathing test and 720 μg after the harsh conditions. In $G^+$ filters, the breathing test displays 10 mg/L, being all organic carbon, which indicates a release of 592 μg for each filter. In contrast, the harsh condition sample shows 645 mg/L of organic carbon, corresponding to 12.9 mg of carbon detached for each filter. Finally, the residues of the FFP2 filters after the breathing and the harsh condition tests contain 15.1 mg/L and 17 mg/L of carbon, respectively, being all organic carbon in these cases. Thus, the amount of organic carbon released in the breathing test was 895 μg and 1.02 mg in the harsh conditions test. Therefore, the quantity of carbon released in the breathing test is similar for the filters with and without graphene. However, when the filters

are submitted to harsh working conditions, the residue of the SHC G@PP, FFP2 and $G^+$ filters present a concentration of organic carbon higher or much higher in the $G^+$ filters case than the residue of the BG-KN95 G@PP filter.

As TOC does not differentiate between graphene and PP, the residues were also analyzed by mass spectrometry to identify the origin of the carbon. The MALDI-TOF mass spectra of all the samples exhibit an intensive peak at *m/z* 478 or 502, which corresponds to a PP fragmentation and shows the expected isotopic distribution (Figs. S18–21). Moreover, for the most concentrated samples (higher TOC), a typical repetitive polymer behavior at higher *m/z* values can be seen [46,47], which also follows the PP distribution (Figs. S20–21), indicating that the organic carbon detected by TOC corresponds to PP. Importantly, the amount of carbon released in both the breathing test and the harsh conditions is similar or even less for the G@PP filters of the BG-KN95 and SHC masks than conventional FFP2 filters, suggesting that the presence of graphene as a composite can improve the stability of the PP filters. Moreover, it is noteworthy that the amount released after the harsh working conditions is significantly lower for the BG-KN95 G@PP case, pointing out that these G@PP composites present more stability than the other.

To confirm that all carbon released is PP, we evaluated the residues by two techniques used to detect graphene. Firstly, UV-VIS spectroscopy was used because graphene presents a characteristic band at 269 nm [36]. However, the BG-KN95 breathing test residue UV–vis spectrum does not reveal any significant signal (Fig. 4a, red line), suggesting that there is no graphene or that it is present in very low concentration. Then, LPE graphene prepared by the method reported by Zamora et al. [36], was used as a fiducial sample to determine the minimum graphene concentration detectable by this technique (Experimental section for details). The reference sample was diluted until no appreciable signal (Fig. 4b), and as a result, *ca.* 1 mg/L was estimated as the detection limit of the equipment. The difference between the UV–vis signals of the residue and the graphene suspension is appreciable with a concentration of 1 mg/L (Fig. 4a black and red lines, respectively). Considering the filter area used and the residue volume, the maximum undetectable graphene weight that each mask might lose is *ca.* 30 μg. Additionally, the Milli-Q water used to sonicate the BG-KN95 G@PP filters was measured by UV–vis. In this case, the UV–vis spectrum also did not present any significant signal (Fig. 4a green line). In this second experiment, the whole G@PP filters of five face masks were used, and the residue was collected in 300 mL. Therefore, the maximum undetectable graphene weight that each mask might lose in the second test is *ca.* 60 μg. The residues of SHC and $G^+$ filters were also measured after the breathing test, and they did not present any significant signal (Fig. 4a pink and brown lines, respectively). By contrast, the residues from harsh working conditions show a small signal at 269 nm, indicating a low detachment of graphene particles (Fig. 4a blue and orange lines).

Additionally, we tried to detect if there were any particles and their size by dynamic light scattering (DLS). This technique is based on the movement of particles in suspension. This movement *versus* time describes an exponential decay that can be correlated with particle size [48]. If there are no particles in suspension or their concentration is below the detection limits of the equipment, and the measured DLS signal is flat. This flat signal is observed in both the residues of experiments that were measured (Fig. 4c red and green lines). As with the other two techniques, we used an LPE graphene sample with a known concentration to determine the detection limit of the equipment, being the lower concentration detectable 0.025 mg/L (Fig. 4d black line). Therefore, this technique suggests that, in the breathing test, the maximum graphene amount that could be detached from each face mask is 0.74 μg, and in the harsh conditions test 1.5 μg. Please note that these estimated values are even lower than the values estimated by UV–vis spectroscopy. This technique also analyzed the residues of the SHC and $G^+$ filters of both experimental conditions. In all the cases, exponential decay is shown (Fig. 4c), confirming the presence of detached particles in the residue.

Besides, the quantities of carbon determined by TOC are much higher than the detection limit of graphene on the other techniques used in this study. Therefore, the organic carbon for BG-KN95 experiments cannot be graphene; otherwise, we would have detected it. These values are much lower than those reported by Shin et al. (9.9 μg of inhaled graphene per day) [30], in which they did not observe damage to the lungs. Therefore, our experiments suggest that BG-KN95 masks are safe for human use. Nevertheless, other commercially available G@PP filters, such as the SHC masks and $G^+$ filters, do not present the same stability, suffering graphene detachment during the tests. Thus, our new degradations tests can complement the present standard methods to ensure the security of the new filters composed of nanomaterials.

## 4. Conclusion

Endurance tests have been carried out on the G@PP composite filters of the BG-KN95 masks, SHC and $G^+$ filters, and on the inner filter of a standard FFP2 mask, introducing a new necessary methodology to characterize the structural endurance and degradation of fibers of sanitary masks, conventional or fabricated using new filters with composites or nanomaterials. These tests have been carried out simulating the human breath during exercise and under harsh working conditions: 8 h, 50 °C, 100% relative humidity, applying more than 5 times more energy than the estimated total energy cost of breathing.

The analyses include morphological characterization of filter fibers, showing that the fiber network, the diameter of the fibers, and the surfaces particles size do not suffer any change after exposure to the experimental conditions. Moreover, a spectroscopic study by Raman mapping was used to confirm that the distribution of the graphene particles along the fiber remains unaltered. In addition, the Raman spectroscopical analysis suggests that the PP morphology does not suffer modification during the tests. Additionally, the graphene and rGO particles of the BG-KN95 and SHC do not present alterations in their structures. Still, some defects were induced on the physical exfoliated graphene of the $G^+$ filters after the tests. Besides, the MALDI-TOF study of the residues reveals that some PP is released during the tests, since the TOC analysis shows that the amount of total carbon present in the residues is similar for both or even less for the G@PP filters than conventional FFP2 filters, suggesting that graphene can provide stability to the PP filters. Furthermore, a battery of techniques (optical and scanning electron microscopy, UV–vis, Raman, and dynamic light scattering) has been used to detect the possible degradation of the fibers that, could lead to harm to human health.

Thus, in this work, we provide a set of tools to evaluate the stability of some filters modified with graphene, showing that the mask's security does not depend only on the presence or absence of graphene but on the structure of the filter. Therefore, these new experimental setups could be an additional ~~different~~ methodology to that used in the UNE standard to ensure the security of the new filters composed of novel composites based on nanomaterials.

## CRediT authorship contribution statement

**Iñigo Torres:** methodology, investigation, writing – original draft. **Brais González-Tobío:** investigation. **Pablo Ares:** supervision, writing – review & editing. **Julio Gómez-Herrero:**

supervision, writing – review & editing. **Félix Zamora:** conceptualization, supervision, writing – review & editing, funding acquisition.

## Declaration of competing interest

The authors declare that they have no known competing financial interests or personal relationships that could have appeared to influence the work reported in this paper.

## Data availability

No data was used for the research described in the article.

## Acknowledgments

We thank Ministerio de Ciencia e Innovacion (projects PID2019-106268GB-C31 and PID2019-106268GB-C32), the financial support through the "María de Maeztu" Programme for Units of Excellence in R&D (CEX2018-000805-M) and Banco de Santander CRUE (Fondo Supera COVID-19).

## Appendix A. Supplementary data

Supplementary data to this article can be found online at https://doi.org/10.1016/j.mtchem.2022.101146.

## References

[1] M.G. Mateu, Structure and Physics of Viruses: an Integrated Textbook, Springer Netherlands, 2013.
[2] S.J. Flint, L.W. Enquist, V.R. Racaniello, A.M. Shalka, Principles of Virology: Molecular Biology, Pathogenesis, and Control of Animal Viruses, ASM Press, 2004.
[3] M.G. Mateu, Assembly, stability and dynamics of virus capsids, Arch. Biochem. Biophys. 531 (2013) 65–79, https://doi.org/10.1016/j.abb.2012.10.015.
[4] J.E. Crowe, Human Respiratory Viruses, 3rd ed., Elsevier, 2008.
[5] J. Gralton, E. Tovey, M.-L. McLaws, W.D. Rawlinson, The role of particle size in aerosolised pathogen transmission: a review, J. Infect. 62 (2011) 1–13, https://doi.org/10.1016/j.jinf.2010.11.010.
[6] L. Morawska, J. Cao, Airborne transmission of SARS-CoV-2: the world should face the reality, Environ. Int. 139 (2020), 105730, https://doi.org/10.1016/j.envint.2020.105730.
[7] M. Jayaweera, H. Perera, B. Gunawardana, J. Manatunge, Transmission of COVID-19 virus by droplets and aerosols: a critical review on the unresolved dichotomy, Environ. Res. 188 (2020), 109819, https://doi.org/10.1016/j.envres.2020.109819.
[8] N. van Doremalen, T. Bushmaker, D.H. Morris, M.G. Holbrook, A. Gamble, B.N. Williamson, T. Azaibi, J.L. Harcourt, N.J. Thornburg, S.I. Gerber, J.O. Lloyd-Smith, E. de Wit, Aerosol and surface stability of SARS-CoV-2 as compared with SARS-CoV-1, N. Engl. J. Med. 382 (2020) 1564–1567, https://doi.org/10.1056/NEJMc2004973.
[9] A. Prather Kimberly, C. Wang Chia, T. Schooley Robert, Reducing transmission of SARS-CoV-2, Science 368 (2020) 1422–1424, https://doi.org/10.1126/science.abc6197.
[10] L.K. Pandey, V.V. Singh, P.K. Sharma, D. Meher, U. Biswas, M. Sathe, K. Ganesan, V.B. Thakare, K. Agarwal, Screening of core filter layer for the development of respiratory mask to combat COVID-19, Sci. Rep. 11 (2021), 10187, https://doi.org/10.1038/s41598-021-89503-x.
[11] I. Soltani, C.W. Macosko, Influence of rheology and surface properties on morphology of nanofibers derived from islands-in-the-sea meltblown nonwovens, Polymer 145 (2018) 21–30, https://doi.org/10.1016/j.polymer.2018.04.051.
[12] A. Brochocka, A. Nowak, K. Majchrzycka, M. Puchalski, S. Sztajnowski, Multifunctional polymer composites produced by melt-blown technique to use in filtering respiratory protective devices, Materials 13 (2020) 712, https://doi.org/10.3390/ma13030712.
[13] L. Bonetti, A. Fiorati, A. Serafini, G. Masotti, F. Tana, A. D'Agostino, L. Draghi, L. Altomare, R. Chiesa, S. Farè, M. Bianchi, L.G. Rizzi, L. De Nardo, Graphene nanoplatelets composite membranes for thermal comfort enhancement in performance textiles, J. Appl. Polym. Sci. 138 (2021), 49645, https://doi.org/10.1002/app.49645.
[14] Z. Han, X. Xiao, H. Qu, M. Hu, C. Au, A. Nashalian, X. Xiao, Y. Wang, L. Yang, F. Jia, T. Wang, Z. Ye, P. Servati, L. Huang, Z. Zhu, J. Tang, J. Chen, Ultrafast and selective nanofiltration enabled by graphene oxide membranes with unzipped carbon nanotube networks, ACS Appl. Mater. Interfaces 14 (2022) 1850–1860, https://doi.org/10.1021/acsami.1c17201.
[15] Z. Zhang, X. Xiao, Y. Zhou, L. Huang, Y. Wang, Q. Rong, Z. Han, H. Qu, Z. Zhu, S. Xu, J. Tang, J. Chen, Bioinspired graphene oxide membranes with pH-responsive nanochannels for high-performance nanofiltration, ACS Nano 15 (2021) 13178–13187, https://doi.org/10.1021/acsnano.1c02719.
[16] V. Palmieri, F. De Maio, M. De Spirito, M. Papi, Face masks and nanotechnology: keep the blue side up, Nano Today 37 (2021), 101077, https://doi.org/10.1016/j.nantod.2021.101077.
[17] F. De Maio, V. Palmieri, G. Babini, A. Augello, I. Palucci, G. Perini, A. Salustri, P. Spilman, M. De Spirito, M. Sanguinetti, G. Delogu, L.G. Rizzi, G. Cesareo, P. Soon-Shiong, M. Sali, M. Papi, Graphene nanoplatelet and graphene oxide functionalization of face mask materials inhibits infectivity of trapped SARS-CoV-2, iScience 24 (2021), 102788, https://doi.org/10.1016/j.isci.2021.102788.
[18] H.M. Hegab, A. ElMekawy, L. Zou, D. Mulcahy, C.P. Saint, M. Ginic-Markovic, The controversial antibacterial activity of graphene-based materials, Carbon 105 (2016) 362–376, https://doi.org/10.1016/j.carbon.2016.04.046.
[19] P. Innocenzi, L. Stagi, Carbon-based antiviral nanomaterials: graphene, C-dots, and fullerenes. A perspective, Chem. Sci. 11 (2020) 6606–6622, https://doi.org/10.1039/D0SC02658A.
[20] L. Huang, M. Gu, Z. Wang, T.W. Tang, Z. Zhu, Y. Yuan, D. Wang, C. Shen, B.Z. Tang, R. Ye, Highly efficient and rapid inactivation of Coronavirus on nonmetal hydrophobic laser-induced graphene in mild conditions, Adv. Funct. Mater. 31 (2021), 2101195, https://doi.org/10.1002/adfm.202101195.
[21] G. Seo, G. Lee, M.J. Kim, S.-H. Baek, M. Choi, K.B. Ku, C.-S. Lee, S. Jun, D. Park, H.G. Kim, S.-J. Kim, J.-O. Lee, B.T. Kim, E.C. Park, S.I. Kim, Rapid detection of COVID-19 causative virus (SARS-CoV-2) in human nasopharyngeal swab specimens using field-effect transistor-based biosensor, ACS Nano 14 (2020) 5135–5142, https://doi.org/10.1021/acsnano.0c02823.
[22] A. Gupta, C.P. Sharma, C. Thamaraiselvan, L. Pisharody, C.D. Powell, C.J. Arnusch, Low-voltage bacterial and viral killing using laser-induced graphene-coated non-woven air filters, ACS Appl. Mater. Interfaces 13 (2021) 59373–59380, https://doi.org/10.1021/acsami.1c20198.
[23] S. Bhattacharjee, R. Joshi, A.A. Chughtai, C.R. Macintyre, Graphene modified multifunctional personal protective clothing, Adv. Mater. Interfaces 6 (2019), 1900622, https://doi.org/10.1002/admi.201900622.
[24] L. Huang, S. Xu, Z. Wang, K. Xue, J. Su, Y. Song, S. Chen, C. Zhu, B.Z. Tang, R. Ye, Self-reporting and photothermally enhanced rapid bacterial killing on a laser-induced graphene mask, ACS Nano 14 (2020) 12045–12053, https://doi.org/10.1021/acsnano.0c05330.
[25] H. Zhong, Z. Zhu, J. Lin, C.F. Cheung, V.L. Lu, F. Yan, C.-Y. Chan, G. Li, Reusable and recyclable graphene masks with outstanding superhydrophobic and photothermal performances, ACS Nano 14 (2020) 6213–6221, https://doi.org/10.1021/acsnano.0c02250.
[26] Z. Lin, Z. Wang, X. Zhang, D. Diao, Superhydrophobic, photo-sterilize, and reusable mask based on graphene nanosheet-embedded carbon (GNEC) film, Nano Res. 14 (2021) 1110–1115, https://doi.org/10.1007/s12274-020-3158-1.
[27] X. Shan, H. Zhang, C. Liu, L. Yu, Y. Di, X. Zhang, L. Dong, Z. Gan, Reusable self-sterilization masks based on electrothermal graphene filters, ACS Appl. Mater. Interfaces 12 (2020) 56579–56586, https://doi.org/10.1021/acsami.0c16754.
[28] F. Seidi, C. Deng, Y. Zhong, Y. Liu, Y. Huang, C. Li, H. Xiao, Functionalized masks: powerful materials against COVID-19 and future pandemics, Small 17 (2021), 2102453, https://doi.org/10.1002/smll.202102453.
[29] A.F. Rodrigues, L. Newman, D. Jasim, S.P. Mukherjee, J. Wang, I.A. Vacchi, C. Ménard-Moyon, A. Bianco, B. Fadeel, K. Kostarelos, C. Bussy, Size-dependent pulmonary impact of thin graphene oxide sheets in mice: toward safe-by-design, Adv. Sci. 7 (2020), 1903200, https://doi.org/10.1002/advs.201903200.
[30] J.H. Shin, S.G. Han, J.K. Kim, B.W. Kim, J.H. Hwang, J.S. Lee, J.H. Lee, J.E. Baek, T.G. Kim, K.S. Kim, H.S. Lee, N.W. Song, K. Ahn, I.J. Yu, 5-Day repeated inhalation and 28-day post-exposure study of graphene, Nanotoxicology 9 (2015) 1023–1031, https://doi.org/10.3109/17435390.2014.998306.
[31] J.K. Kim, J.H. Shin, J.S. Lee, J.H. Hwang, J.H. Lee, J.E. Baek, T.G. Kim, B.W. Kim, J.S. Kim, G.H. Lee, K. Ahn, S.G. Han, D. Bello, I.J. Yu, 28-Day inhalation toxicity of graphene nanoplatelets in Sprague-Dawley rats, Nanotoxicology 10 (2016) 891–901, https://doi.org/10.3109/17435390.2015.1133865.
[32] L. Amendola, M.T. Saurini, F. Di Girolamo, F. Arduini, A rapid screening method for testing the efficiency of masks in breaking down aerosols, Microchem. J. 157 (2020), 104928, https://doi.org/10.1016/j.microc.2020.104928.
[33] M. Joshi, A. Khan, B.K. Sapra, Quick laboratory methodology for determining the particle filtration efficiency of face masks/respirators in the wake of COVID-19 pandemic, J. Ind. Textil. 51 (5S) (2020) 7622S–7640S, https://doi.org/10.1177/1528083720975084.
[34] A. Konda, A. Prakash, G.A. Moss, M. Schmoldt, G.D. Grant, S. Guha, Aerosol filtration efficiency of common fabrics used in respiratory cloth masks, ACS Nano 14 (2020) 6339–6347, https://doi.org/10.1021/acsnano.0c03252.
[35] E. Vo, M. Horvatin, M. Bergman, B. Wu, Z. Zhuang, A technique to measure respirator protection factors against aerosol particles in simulated workplace settings using portable instruments, J. Occup. Environ. Hyg. 17 (2020) 231–242, https://doi.org/10.1080/15459624.2020.1735640.
[36] M.-R. Azani, A. Hassanpour, V. Carcelén, C. Gibaja, D. Granados, R. Mas-Ballesté, F. Zamora, Highly concentrated and stable few-layers graphene suspensions in pure and volatile organic solvents, Appl. Mater. Today 2 (2016) 17–23, https://doi.org/10.1016/j.apmt.2015.12.002.

[37] L. Int Panis, B. de Geus, G. Vandenbulcke, H. Willems, B. Degraeuwe, N. Bleux, V. Mishra, I. Thomas, R. Meeusen, Exposure to particulate matter in traffic: a comparison of cyclists and car passengers, Atmos. Environ. 44 (2010) 2263–2270, https://doi.org/10.1016/j.atmosenv.2010.04.028.
[38] S. Choi, R. Park, N. Hur, W. Kim, Evaluation of wearing comfort of dust masks, PLoS One 15 (2020), e0237848, https://doi.org/10.1371/journal.pone.0237848.
[39] A.C. Ferrari, J.C. Meyer, V. Scardaci, C. Casiraghi, M. Lazzeri, F. Mauri, S. Piscanec, D. Jiang, K.S. Novoselov, S. Roth, A.K. Geim, Raman spectrum of graphene and graphene layers, Phys. Rev. Lett. 97 (2006), 187401, https://doi.org/10.1103/PhysRevLett.97.187401.
[40] U. Khan, A. O'Neill, M. Lotya, S. De, J.N. Coleman, High-concentration solvent exfoliation of graphene, Small 6 (2010) 864–871, https://doi.org/10.1002/smll.200902066.
[41] S. Haar, M. El Gemayel, Y. Shin, G. Melinte, M.A. Squillaci, O. Ersen, C. Casiraghi, A. Ciesielski, P. Samorì, Enhancing the liquid-phase exfoliation of graphene in organic solvents upon addition of n-Octylbenzene, Sci. Rep. 5 (2015), 16684, https://doi.org/10.1038/srep16684.
[42] G. Liu, J. Chen, X. Hou, W. Huang, A highly-sensitive electrochemical sensor for the simultaneous detection of Cd2+ and Pb2+ using liquid phase-exfoliated graphene, Anal. Methods 6 (2014) 5760–5765, https://doi.org/10.1039/C4AY00405A.
[43] N.M.S. Hidayah, W.-W. Liu, C.-W. Lai, N.Z. Noriman, C.-S. Khe, U. Hashim, H.C. Lee, Comparison on graphite, graphene oxide and reduced graphene oxide: synthesis and characterization, AIP Conf. Proc. 1892 (2017), 150002. https://aip.scitation.org/doi/abs/10.1063/1.5005764.
[44] S. Thakur, N. Karak, Green reduction of graphene oxide by aqueous phytoextracts, Carbon 50 (2012) 5331–5339, https://doi.org/10.1016/j.carbon.2012.07.023.
[45] I. Bisutti, I. Hilke, M. Raessler, Determination of total organic carbon – an overview of current methods, TrAC, Trends Anal. Chem. 23 (2004) 716–726, https://doi.org/10.1016/j.trac.2004.09.003.
[46] J. Horský, Z. Walterová, Fingerprint multiplicity in MALDI-TOF mass spectrometry of copolymers, Macromol. Symp. 339 (2014) 9–16, https://doi.org/10.1002/masy.201300122.
[47] P. Rizzarelli, S. Carroccio, Modern mass spectrometry in the characterization and degradation of biodegradable polymers, Anal. Chim. Acta 808 (2014) 18–43, https://doi.org/10.1016/j.aca.2013.11.001.
[48] B.J. Berne, R. Pecora, Dynamic Light Scattering: with Applications to Chemistry, Biology, and Physics, Courier Corporation, 2013.